



HAL
open science

Electrodeposition of polymer electrolyte into carbon nanotube tissues for high performance flexible Li-ion microbatteries

Florence Vacandio, Vinsensia Ade Sugiawati, Yair Ein-eli, Thierry Djenizian

► **To cite this version:**

Florence Vacandio, Vinsensia Ade Sugiawati, Yair Ein-eli, Thierry Djenizian. Electrodeposition of polymer electrolyte into carbon nanotube tissues for high performance flexible Li-ion microbatteries. *APL Materials*, 2019, 7 (3), pp.031506. 10.1063/1.5082837. hal-02649660

HAL Id: hal-02649660

<https://amu.hal.science/hal-02649660>

Submitted on 29 May 2020

HAL is a multi-disciplinary open access archive for the deposit and dissemination of scientific research documents, whether they are published or not. The documents may come from teaching and research institutions in France or abroad, or from public or private research centers.

L'archive ouverte pluridisciplinaire **HAL**, est destinée au dépôt et à la diffusion de documents scientifiques de niveau recherche, publiés ou non, émanant des établissements d'enseignement et de recherche français ou étrangers, des laboratoires publics ou privés.



Distributed under a Creative Commons Attribution 4.0 International License

Electrodeposition of polymer electrolyte into carbon nanotube tissues for high performance flexible Li-ion microbatteries

Cite as: APL Mater. 7, 031506 (2019); <https://doi.org/10.1063/1.5082837@apm.2019.FLEX2019.issue-1>
Submitted: 25 November 2018 . Accepted: 23 December 2018 . Published Online: 13 February 2019

Vinsensia Ade Sugiawati , Florence Vacandio , Yair Ein-Eli , and Thierry Djenizian 

COLLECTIONS

Paper published as part of the special topic on [Advances in Flexible and Soft Electronics](#) and [Collection](#)



View Online



Export Citation



CrossMark

ARTICLES YOU MAY BE INTERESTED IN

[Electrodeposition of polymer electrolyte into carbon nanotube tissues for high performance flexible Li-ion microbatteries](#)

APL Materials 7, 031506 (2019); <https://doi.org/10.1063/1.5082837>

ORDER PRINT EDITION



AIP Conference Proceedings

**The 18th International Conference
on Positron Annihilation**

Electrodeposition of polymer electrolyte into carbon nanotube tissues for high performance flexible Li-ion microbatteries

Cite as: APL Mater. 7, 031506 (2019); doi: 10.1063/1.5082837
Submitted: 25 November 2018 • Accepted: 23 December 2018 •
Published Online: 13 February 2019



Vinsensia Ade Sugiawati,¹  Florence Vacandio,¹  Yair Ein-Eli,²  and Thierry Djenizian^{3,a)} 

AFFILIATIONS

¹CNRS, Electrochemistry of Materials Research Group, MADIREL, UMR 7246, Aix Marseille Université, F-13397 Marseille Cedex 20, France

²Department of Materials Science and Engineering, The Nancy and Stephan Grand Technion Energy Program, Technion-Israel Institute of Technology, Haifa 3200003, Israel

³Department of Flexible Electronics, Center of Microelectronics in Provence, Mines Saint-Etienne, F-13541 Gardanne, France

^{a)} Author to whom correspondence should be addressed: thierry.djenizian@emse.fr

ABSTRACT

Polymer-coated Carbon Nanotube (CNT) tissues are very flexible and lightweight and have high potential as an anode material for flexible Li-ion microbatteries. The electrochemical deposition of p-sulfonated poly(allyl phenyl ether) (SPAPE) polymer electrolyte into CNT tissues has been accomplished using a cyclic voltammetry (CV) technique. When compared to a pristine CNT tissue, the capacity of SPAPE-coated CNT tissue after 10 cycles of CV is improved about 67% at 1C rate. The enhancement of electrochemical performance is obtained when the CNT tissues are coated with the SPAPE polymer electrolyte. The higher capacity of the SPAPE-coated CNT tissue is attributed to the increased surface area and the improved quality of the electrode/electrolyte interfaces between the nanotubes and the polymer electrolyte. The SPAPE-coated CNT tissue delivers a higher reversible capacity of 750 mAh g⁻¹ (276 μAh cm⁻²) compared to a pristine CNT tissue, which solely provides a reversible capacity of 450 mAh g⁻¹ (166 μAh cm⁻²) after 110 cycles at 1C rate. Remarkably, the SPAPE-coated CNT tissue reaches a high capacity up to 12C rate while observing that the capacity can be significantly recovered.

© 2019 Author(s). All article content, except where otherwise noted, is licensed under a Creative Commons Attribution (CC BY) license (<http://creativecommons.org/licenses/by/4.0/>). <https://doi.org/10.1063/1.5082837>

Due to its excellent properties such as high energy and power density, low self-discharge, long cycle life, almost no memory effect, and high working voltage, lithium-ion batteries (LIBs) play an important role in various applications such as grid energy storage, electric vehicles, microelectronics, etc.^{1,2} Despite being commercially successful, some remaining challenges for the future generation of lightweight, thin, and flexible LIBs are still under investigation.^{3,4} More interest in flexible LIBs as power sources is growing in order to meet the requirements of modern devices and emerging technologies such as implanted medical devices, integrated circuit smart cards, flexible electronics, radio-frequency identification devices (RFIDs), and wearable devices.^{5,6}

Typically, LIBs consist of a cathode and an anode separated by a separator, which is soaked in an electrolyte solution. Both electrodes are prepared via a slurry casting method containing the active material powder mixed with a binder polymer such as polyvinylidene fluoride (PVDF) and carbon black as a conductive agent. The slurry is then casted onto metal foils as current collectors such as copper and aluminum. However, this type of composite electrode is not compatible for flexible LIBs due to weak adhesion between the active layer and the current collector. Besides its weak adhesion, the active material layer will also be damaged or peeled off easily from the current collector, thereby reducing the overall energy density of LIBs.⁷

A number of studies have been conducted aiming to find promising electrode materials, striving toward high performance flexible LIBs. Recently, considerable research efforts have explored the electrode materials for flexible LIBs such as carbon nanotubes (CNTs),⁸ carbon nanofibers,^{9,10} nanowires,^{11,12} graphene,¹³ and so forth. Among them, CNT tissues possess unique and outstanding properties such as low density, high electrical and thermal conductivity, excellent mechanical properties, high flexibility, and low cost.^{5,14–16} The electrochemical reactivity and porosity make CNT tissues an attractive host material for energy storage applications.¹⁷ In addition, CNT tissues can be easily shaped into various forms and configuration in different applications of flexible and lightweight electronic devices. Many efforts have been made to synthesize the CNT electrodes aiming to replace the graphite-based anodes. For example, Gao *et al.* synthesized a CNT multiple-layer film in a vertical Chemical Vapour Deposition (CVD) gas flow reactor.¹⁸ Also, Yang *et al.* synthesized short CNTs by the co-pyrolysis method and long CNTs by a CVD technique. Their electrochemical performances were compared, and it was found that the reversible capacity of short CNT is almost twice larger than that of long CNT.¹⁹

To fabricate all-solid-state Li-ion microbatteries, solid electrolytes such as polymer electrolyte have drawn major attention in order to avoid the leakage risk. Polymer electrolytes have been considered to be a safe alternative as a replacement of conventional liquid electrolytes in Li-ion microbatteries, and major progress has been made to fulfill these requirements.^{20–22} More recently, our group has reported the electrochemical synthesis of p-sulfonated poly(allyl phenyl ether) (SPAPE) as the polymer electrolyte on titanium dioxide nanotube (TiO₂nt) electrodes using the cyclic voltammetry (CV) technique. The results showed an excellent improvement of the areal capacity with a very good capacity retention.²³ In this present work, we study the electrodeposition of SPAPE polymer electrolyte onto CNT tissues as the anode material. The electrochemical characterizations show that the electropolymerized coating material has a significant positive influence on the electrochemical performance of the CNT electrodes.

CNT tissues with a thickness of 30 μm were received from Tortech nano Fibers Ltd. (Israel) and were washed pre-treated in iso-propyl alcohol, as reported elsewhere.^{24,25} This type of CNT tissues has a porosity of 70%–80% and a density of 0.613 g cm^{-3} .²⁴ Cu film was deposited onto the CNT tissues by RF sputtering (MP300 model, PLASSYS) with the use of a Cu target (purity: 99.9%, Neyco). The sputtering process was carried out immediately in a vacuum chamber with a base pressure of 3×10^{-6} mbar prior to deposition. The sputtering gas used was pure argon with a working pressure of 10 mTorr and a gas flow of 21.5 sccm. A sputtering power of 150 W for 30 min was applied to deposit a 300 nm-thin Cu layer acting as both the backside connection for the electrochemical deposition and the anode current collector.

Cyclic Voltammetry (CV) was performed onto the CNT tissues in order to polymerize the sulfonated aromatic precursor. An electrolyte solution containing 5.2×10^{-3} M of

the synthesized monomer was mixed with 0.5 M lithium-bis(trifluoromethane)sulfonimide (LiTFSI, Sigma Aldrich) as a supporting electrolyte and dimethylsulfoxide (DMSO, Sigma Aldrich) as a solvent. More details regarding the monomer synthesis were described in our earlier report.²³ Prior to electrodeposition, the electrolyte was purged with argon gas for 10 min to remove dissolved oxygen. The CV test was carried out in a three-electrode electrochemical cell with CNT tissues as the working electrode, a platinum sheet as the counter electrode, and saturated Ag/AgCl as the reference electrode. The experiments were performed between -0.9 and -1.8 V vs. Ag/AgCl at a scan rate of 20 mV s^{-1} with a various number of CV cycles such as 5, 10, 50, and 100 cycles. After electrodeposition of polymer electrolyte, the SPAPE-coated CNT was dried in a Buchi vacuum dryer at 70 $^{\circ}\text{C}$ overnight to remove the solvents.

The morphology of the CNT tissues was characterized by using a field-emission scanning electronmicroscope (SEM, Ultra-55 Carl Zeiss) and by Transmission Electron Microscopy (TEM) using a JEOL 2000FX microscope. Pristine CNT and SPAPE-coated CNT (surface area: 0.44 cm^2) were used as electrodes with neither binder nor carbon additives being added. Both CNT electrodes were assembled against a Li foil using a two electrode Swagelok cell. A 9 mm diameter Li foil was used as the reference electrode, and a Whatman glass microfiber separator with a diameter of 10 mm was added between the two electrodes. Cyclic voltammetry experiments were performed using a VMP3 (Bio Logic) in the range of 0.01–2 V vs. Li/Li⁺ with a scan rate of 0.2 mV s^{-1} . Galvanostatic cycles were performed with a VMP3 (Bio Logic) between 0.01 and 2 V vs. Li/Li⁺. The different charge-discharge profiles were obtained by galvanostatic experiments at different C-rates (1C, 2C, 5C, 10C, and 12C). The current densities for the pristine CNT and SPAPE-coated CNT at 1C, 2C, 5C, 10C, and 12C were 0.12, 0.24, 0.60, 1.20, and 1.44 mA cm^{-2} , respectively. All cells were assembled in a glove box, filled with high purity argon in which the oxygen and moisture contents were less than 0.5 ppm.

The CNT tissue [Fig. 1(a)] has been considered as a promising anode material for flexible Li-ion microbatteries owing to its unique structure and properties, along with much improved capacity compared to the graphite anode.^{26,27} In the present work, a Cu metal is deposited onto the CNT tissues through RF sputtering [Fig. 1(b)]. In fact, a Cu foil is the commonly used anode current collector in commercial Li-ion cells because it was found that there is no significant reaction between Li and copper, taking place at low potential of the anode material which is close to 0 vs. Li/Li⁺.²⁸ The thickness of the Cu foils in commercial Li-ion cells has been reported to be 10 μm with an areal density about 10 mg cm^{-2} .²⁹ When compared to a common Cu current collector, the thickness of the sputtered Cu film is much thinner, varying between 250 and 300 nm, as shown in Fig. 1(c). Due to the very thin Cu sputtered coating, the composite [Cu-CNT] tissue remains as the highly flexible material.

In this work, an aromatic polymer has been employed as the electrolyte. As it has been mentioned in the literature, the aromatic polymer films are usually deposited onto a

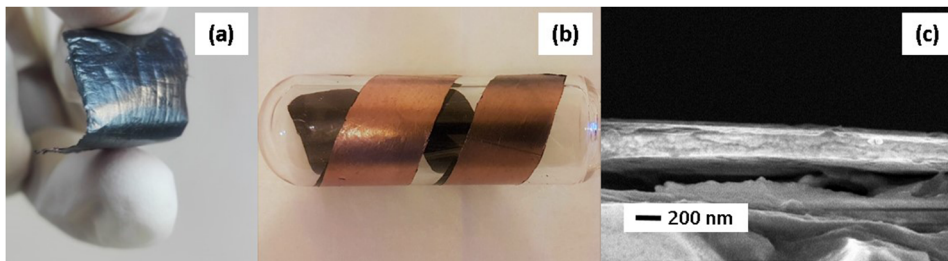


FIG. 1. Photo of the pristine CNT tissue (a), the sputtered Cu thin film deposited on a CNT tissue (b), and the SEM cross-sectional view of the Cu thin film (c).

conductive or semiconductive surface using different electrochemical methods, including potentiostatic, galvanostatic, and potentiodynamic methods.^{23,30,31} Cyclic voltammetry (CV) is one of the most viable route to achieve the electrodeposition of polymers. This method is an effective bottom-up approach to realize the conformal coating of nanostructured electrodes particularly with the polymer electrolyte, as previously reported.^{32,33} In this work, the cyclic voltammetry

technique has been chosen to deposit the polymer electrolyte onto the CNT tissues. As seen in Fig. 2, a typical cyclic voltammogram is presented which is corresponding to the electropolymerization of p-sulfonated (allyl phenyl ether) in cathodic conditions. In this study, electropolymerization was carried out in two different electrolytes in order to observe the effect of the monomer addition. The initial current drops for both electrolyte containing LiTFSI salts with monomers

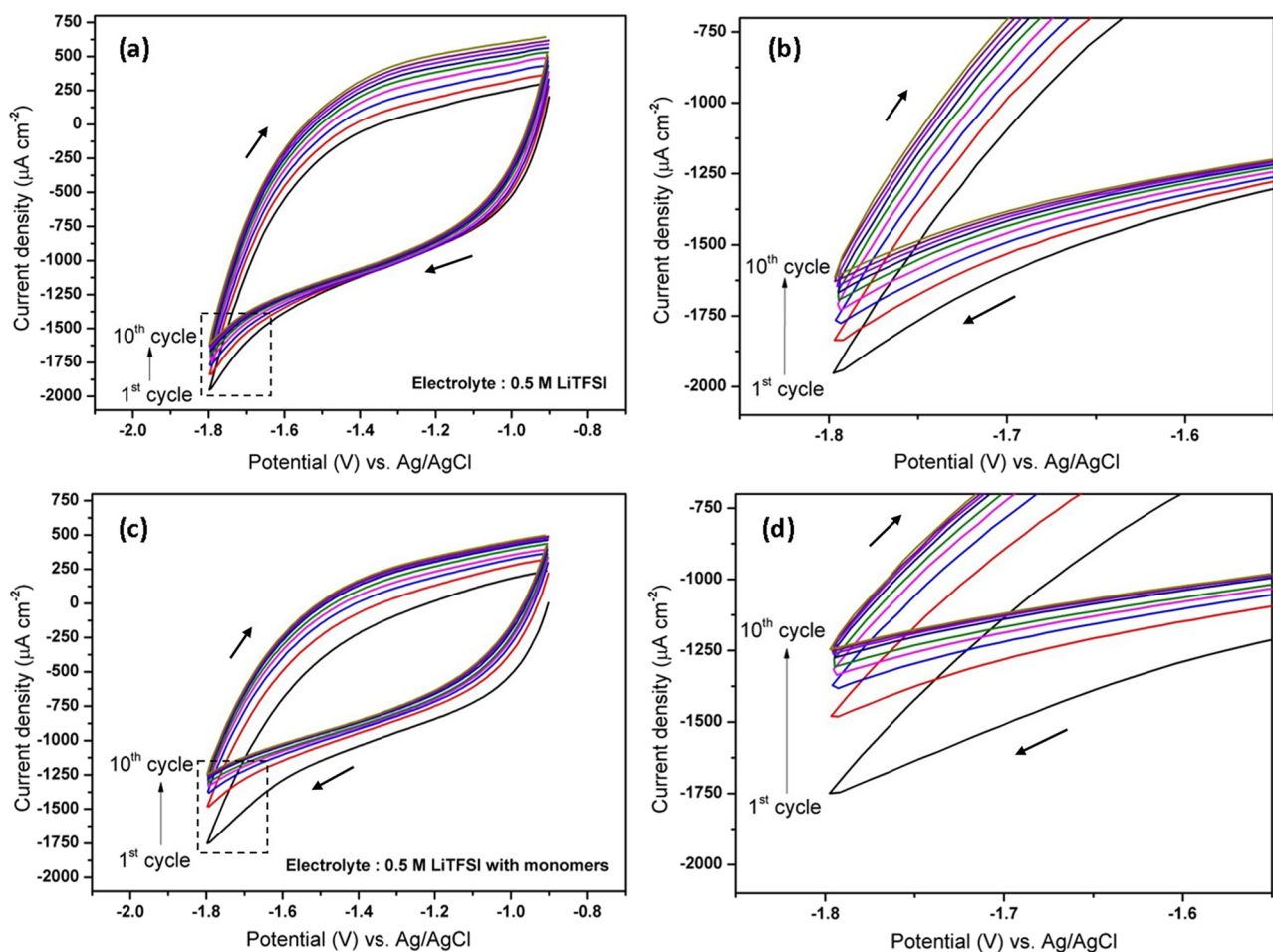


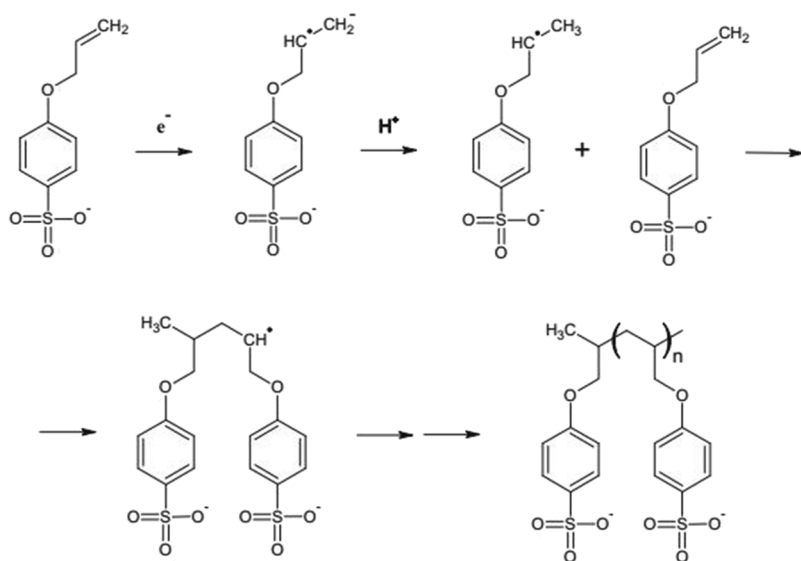
FIG. 2. Cyclic voltammograms of CNT tissues recorded between -0.9 V and -1.8 V vs. Ag/AgCl in 0.5 M LiTFSI [(a) and (b)] and 0.5 M LiTFSI + monomers [(c) and (d)].

and without monomers are observed. It is worth noting that the electrolytes containing volatile solvents with a high vapor pressure and flammability needed a supporting electrolyte such as LiTFSI salts, which is often incorporated into the electrodeposited film.³⁴ It has outstanding electrochemical properties and high intrinsic chemical and thermal stability.³⁵ As can be seen at the cathodic current, a higher current drops between the first and the second cycle at the potential of -1.8 V vs. Ag/AgCl can be clearly found for the monomer-containing electrolyte. The reason for this could be attributed to the formation of an insulator film layer with the increase in the number of cycles. The absolute current density progressively decreases with successive cycles, indicating the electrode is passivated. It is due to the fact that the growth of passive polymer film on the electrode would reduce the electroactive surface area, leading to increase in the electrode resistance. Indeed, the current drops are more pronounced in the initial cycles for the LiTFSI solution carrying the SPAPE monomer compared to without a monomer. Additionally, comparing the CV curves of both electrolytes, no new reduction peaks are observed after adding the monomer. It is assumed that the monomer itself does not undergo direct reduction at the electrode. The optimum number of CV cycles to infiltrate the polymer electrolyte into CNT tissues is determined by accomplishing a series of experiments in which electrodeposition of SPAPE polymer electrolyte is carried out with several number of cycles such as 5, 10, 50, and 100 cycles. However, after 10 cycles of CV, the peak currents reach a saturation condition and the current density does not decrease anymore. It is probably due to the available active surface area of the CNT electrode for the polymer electrolyte deposition is reduced as the number of CV cycles approaches 10 cycles. Therefore, the optimum number of cycles should not be below and above 10 cycles in order to obtain a good polymer film and hence could improve the electrochemical performances of the cells.

Scheme 1 presents the possible pathway for the electropolymerization of p-sulfonated (allyl phenyl ether) in cathodic conditions. The mechanism starts by the electron-transfer step producing the formation of radical anion, and afterwards, a proton from the reaction medium is added to form the more stable secondary radical. The secondary radical reacts with monomers at the electrode surface leading to the formation and deposition of the polymer.²³

The surface morphological analysis before and after electropolymerization was performed by using SEM. The top surfaces of the pristine CNT tissues are shown in **Figs. 3(a)** and **3(b)**. The pristine CNT tissue appears as continuously disoriented curved nanotubes with the average diameter ranges between 5 and 30 nm. The surface of the CNT tissues after 10 cycles shows that the polymer filled the void area from the bottom part of CNT tissues. Therefore, the void area between nanotubes does not appear due to the polymer filling [**Figs. 3(c)** and **3(d)**]. The dense nanotubes due to the presence of polymer electrolyte are confirmed by a cross-sectional view of SPAPE-coated CNT tissue (see **Fig. S1, supplementary material**).

Figure S2 of the **supplementary material** depicts the elemental energy dispersive X-ray (EDX) analysis spectra. The presence of Fe particles (2.13 At. %) on the pristine CNT surfaces is detected which is assumed as an inevitable catalyst residue of metal impurities resulting from the manufacture process.^{24,36} In addition, a very low quantity of Si (0.07 At. %) and S (0.26 At. %) on the CNT tissues before electropolymerization has been detected as the traces of impurities. After electropolymerization, EDX spectra show a strong peak of F (17.83 At. %) and S (6.71 At. %) which is attributed to the polymer layer. Moreover, we also observed that the electropolymerization process allows the formation of densified and bundled CNT tissues due to an interaction existing between the neighboring tubes. Herein, it is assumed that the capillary forces and wetting capability could produce denser



SCHEME 1. Electropolymerization mechanism for p-sulfonated poly(allyl phenyl ether) (SPAPE).

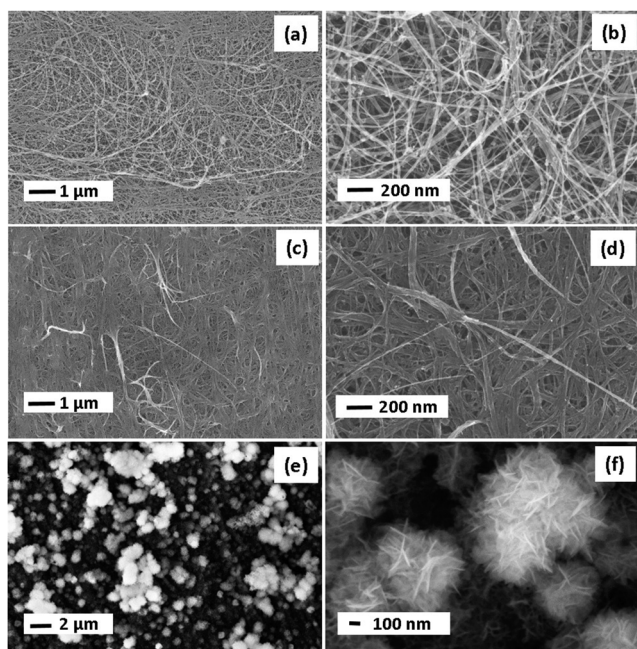


FIG. 3. SEM images of CNT tissues before electropolymerization [(a) and (b)], after electropolymerization for 10 cycles of CV [(c) and (d)], and after electropolymerization for 100 cycles of CV [(e) and (f)].

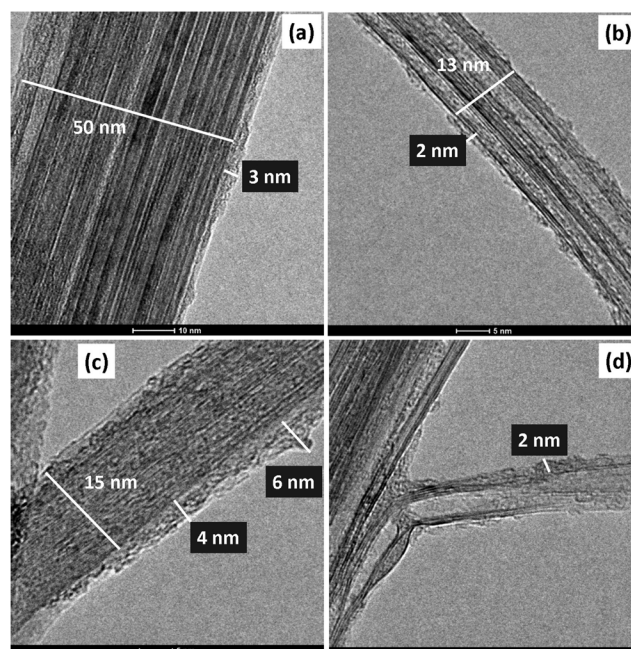


FIG. 4. Transmission electron micrographs of CNT tissues after electropolymerization for 10 cycles [(a) and (b)] and 100 cycles [(c) and (d)].

CNT surfaces due to van der Waals force interaction among nanotubes.^{25,37}

In this study, electropolymerization was performed at different numbers of CV cycles such as 5, 10, 50, and 100 cycles. However, higher cycles lead to the formation of micro-nano particles of Li salts. Presumably, the Li salts start to crystallize after 10 cycles when the CNT surface is already covered by the thin polymer film. After 50 cycles, the surface area of CNT tissues is covered by the polymer film and Li salts (See Fig. S3, [supplementary material](#)). The growth of the Li salts on the whole surface area of CNT occurred after 100 cycles. The diameter of micro-nano particles is ranging from 500 nm to 1.5 μm. Additionally, the tubes are clearly visible after 5 cycles suggesting that the polymer has not penetrated yet on the entire CNT surfaces. Therefore, the optimum polymer covering is estimated to be reached after 10 cycles. It is worth noting that the electrochemical deposition of an ion-conduction polymer is self-limiting owing to its extremely low electronic conductivity. Hence, the growth rate decreases with the increase in the number of CV cycles as well as the blocking takes place when the polymer electrolyte attains a certain thickness of polymer film.²³

TEM characterization is utilized to confirm the presence of polymer film. The TEM analysis reveals the presence of a thin polymer film on the tube walls with a thickness in the order of 2–3 nm for 10 cycles [Figs. 4(a) and 4(b)]. It is assumed that the polymer film is electrodeposited not only on the tube walls but also in the interwall spacing between the tubes. With further increasing CV cycles up to 100 cycles, a thicker film

ranging from 2 to 6 nm is obtained, as shown in Figs. 4(c) and 4(d). Moreover, the TEM results also confirm the bundles and densified CNTs after electropolymerization, for example, 50, 13, and 15 nm are found to be the sizes of several nanotubes which tend to adhere to each other through the van der Waals force. The carbon nanotubes are clearly crystalline as TEM imaging shows linear graphene layers along the tubes. It is important to note that the CNT tissues used in this study are closed carbon nanotubes with the capped tube ends, so it makes the inner core not accessible for the Li⁺ intercalation. As it has been reported, compared to opened carbon nanotubes, the closed CNT with the presence of pentagons and heptagons showed better cycling performances.³⁸

Cyclic voltammetry measurements were performed for the pristine CNT and SPAPE-coated CNT after 10 cycles within a potential range of 0.01–2 V (vs. Li/Li⁺), as presented in Figs. 5(a)–5(d). During the first cycle, both CNT electrodes exhibit sharp cathodic peaks of approximately 0.6 V without any oxidation peaks. These peaks can be attributed to the formation of a Solid Electrolyte Interphase (SEI) on the surface of the CNT electrodes.¹⁴ When compared to pristine CNT, the cathodic peak of the SPAPE-coated CNT reveals a higher absolute current density, which is probably caused by enhancement of the surface contact established between the electrode and the electrolyte owing to the electrodeposited polymer. However, the sharp peak at the first cycle is not apparent in the 2nd, 5th, and 10th cycles, suggesting that a stable SEI is formed after the first cycle. Furthermore, during the 2nd, 5th, and 10th cycles, another reduction peak located at ca. 0.01 V

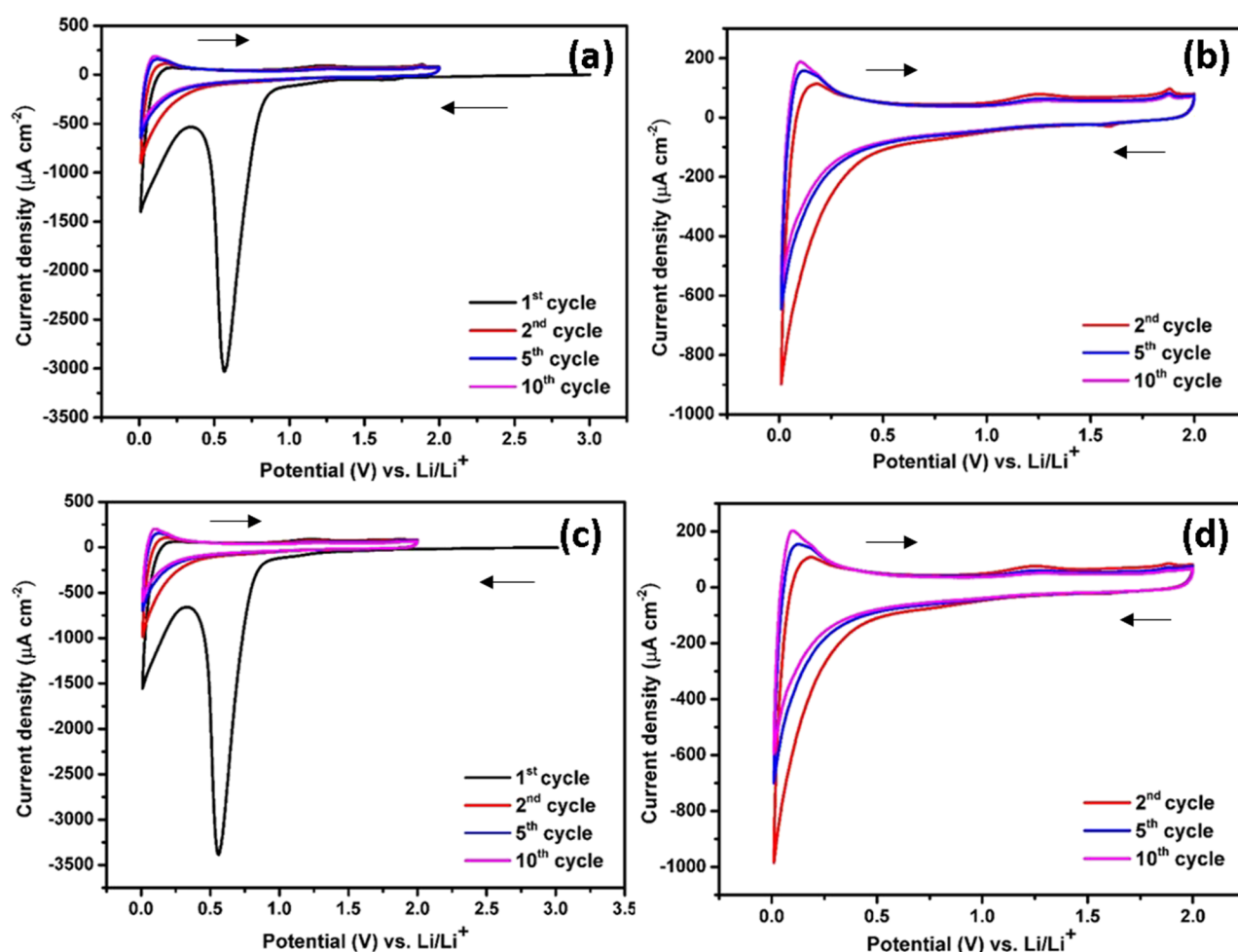


FIG. 5. Cyclic voltammogram of CNT tissues with a scan rate of 0.2 mV s^{-1} before electropolymerization (pristine CNT) [(a) and (b)] and after electropolymerization for 10 cycles [(c) and (d)].

and oxidation peaks at ca. 0.1 V correspond to intercalation and deintercalation of Li ions into CNT tissues. The broad oxidation peaks at ca. 1.25 V are less pronounced, and this corresponds to the intercalation and deintercalation of Li ions into the various cavities existing in the CNT tissues. In addition, the small oxidation peak around 1.8 V might be ascribed to the reaction of lithium with hydrogen functional groups on the CNT surfaces. These findings are in good agreement with the previous report.³⁹

The number of cycles employed to the cell during the electropolymerization process is found affecting the storage performance of the electrochemical cells. In this case, 10 and 100 cycles are selected to compare the effect of thin and thick polymer films. In order to evaluate the electrochemical properties of the three different CNT electrodes including pristine CNT, SPAPE-coated CNT after 10 cycles of CV, and SPAPE-coated CNT after 100 cycles of CV, the three cells were cycled at 1C using galvanostatic charge-discharge tests. Figures 6(a)

and 6(b) show the comparison of the reversible discharge capacities of the pristine CNT ($185 \mu\text{Ah cm}^{-2}$), SPAPE-coated CNT after 10 cycles of CV ($309 \mu\text{Ah cm}^{-2}$), and SPAPE-coated CNT after 100 cycles of CV ($153 \mu\text{Ah cm}^{-2}$) over 30 cycles at 1C rate. The discharge capacities decrease drastically for all the CNT electrodes in the first few cycles, and afterwards, sustainably stable reversible capacities can be reached.

The SPAPE-coated CNT after 100 cycles of CV showed the lowest capacities, meaning the 10 cycles of CV with the thin polymer film is considered to be the optimum condition since the ionic conductivity of the polymer electrolyte at room temperature is lower compared to the common liquid electrolyte. This low ionic conduction should be compensated by minimizing the polymer film thickness to reduce the Li diffusion path length. This is probably the reason why 100 cycles of CV showed the lowest storage capacity among the three CNT electrodes.

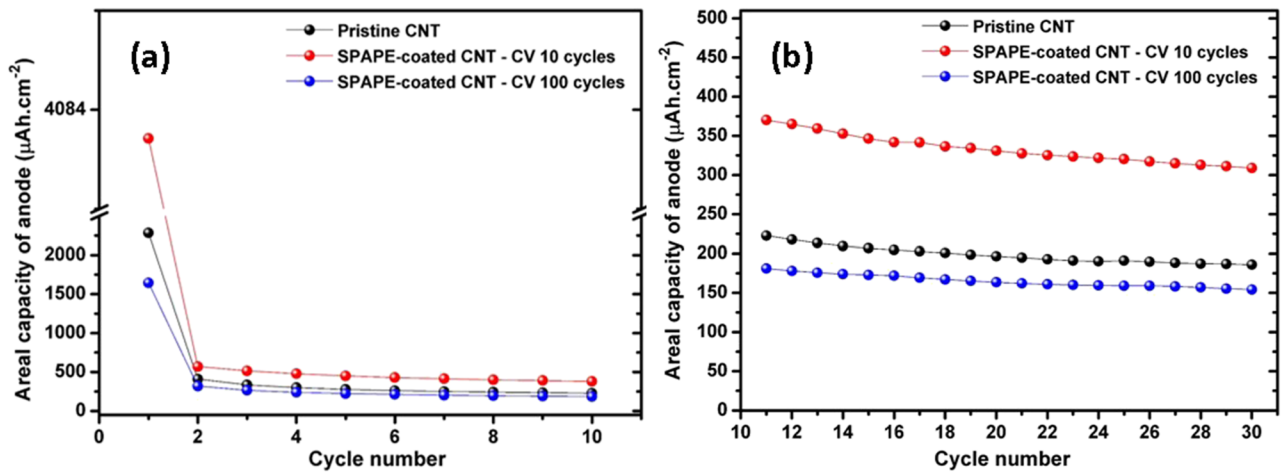


FIG. 6. Comparison of the cycling performance of pristine CNT and SPAPE-coated CNT [(a) and (b)], revealing the superior electrochemical properties of the SPAPE-coated CNT after electropolymerization for 10 cycles.

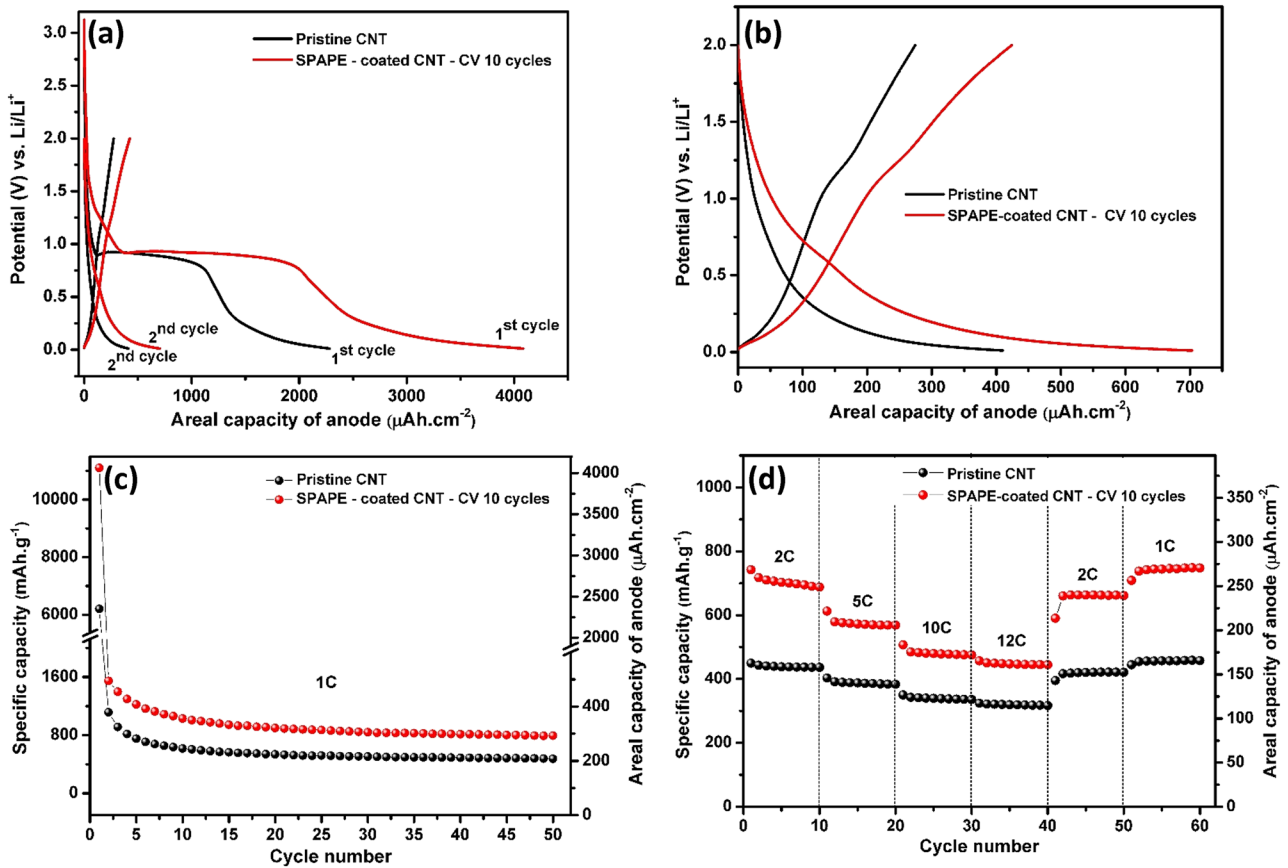


FIG. 7. Galvanostatic charge-discharge profile at the 1st and 2nd cycles at 1C rate (a) and the 2nd cycle at 1C rate (b) and the discharge capacity of Li-ion microbatteries for 50 cycles at 1C rate (c) and multiple C-rates (d).

To further study the influences of the polymer deposition on the electrochemical performance of SPAPE-coated CNT, galvanostatic charge-discharge cycling tests were performed at multiple C-rates in a half cell against the Li foil. Figure 7(a) shows a comparison of the cycling performance of both pristine CNT and SPAPE-coated CNT for 10 cycles of CV. As seen that just after the cell is assembled, the open-circuit cell voltage is close to 3.0 V indicating that the CNT electrode is in the delithiated state. The open circuit voltage is consistent with the CV curve. Upon the first discharge, the cell voltage drops rapidly and forms a plateau of about 0.8 V. This typical plateau is found in most graphite or CNT materials due to the decomposition of electrolyte and the formation of SEI film.^{19,40,41} Moreover, as previously seen from SEM images, the CNT bundles were formed after the electropolymerization, resulting from van der Waals forces between the neighboring tubes. The interstitial spaces of CNT bundles are expected to accommodate the Li ion intercalation, leading to higher storage capacity. Li ions can also penetrate into the interstitial spaces between the neighboring CNT. However, the Li ions located between the neighboring CNT have very strong adsorption potentials, making their removal from the CNT bundles difficult.³⁸ Obviously, the voltage plateau at 0.8 V in the first discharge curve for the SPAPE-coated CNT is longer than that for the pristine CNT. This indicates that the irreversible capacity of the SPAPE-coated CNT is higher than that

of the pristine CNT. It could also be ascribed to the much higher contact between the electrode and the electrolyte of the SPAPE-coated CNT electrode due to the electropolymerization. After the formation of the first plateau, the voltage gradually decreases during the discharge process, and then, the second plateau at ~0.1 V appears in the voltage curve of both electrodes, as presented in Fig. 7(b). Such plateau should be attributed to the intercalation of Li ions into CNT.⁴² Moreover, during the first charge process, there is a plateau around 1.1 V which is assigned to the deintercalation of Li ions between the graphene layers.⁴³ Pristine CNT and SPAPE coated CNT display the similar charge and discharge plateaus. Thus, the intercalation/deintercalation mechanism of Li ions in the two kinds of CNT tissues is similar. For pristine CNT, the irreversible discharge capacity is 6204 mAh g⁻¹ (2281 μAh cm⁻²) and the charge capacity is 748 mAh g⁻¹ (275 μAh cm⁻²), which yields an initial Coulombic efficiency (ICE) of 12%. The SPAPE-coated CNT shows a higher discharge capacity of 11100 mAh g⁻¹ (4083 μAh cm⁻²) and a charge capacity of 1155 mAh g⁻¹ (425 μAh cm⁻²), with an ICE of 10.4%. A very low initial cycle efficiency about 17.3% and a reversible capacity of 135 mAh g⁻¹ have been also previously reported.⁴⁴ Generally, it is a common issue of the nanocarbon electrodes.⁴⁵ Nevertheless, the reduction of high irreversible capacity and a realization of full cell flexible microbatteries utilizing CNT tissues as the flexible anode material are our ongoing research. Additionally, a very

TABLE I. Comparison of the electrochemical performances of various CNTs.

Electrode	Potential window (V vs Li/Li ⁺)	C-rate	Reversible capacity (mAh g ⁻¹)	Gains
SPAPE-coated CNT	0.01-2	1C	750	As reference
		2C	700	
		5C	575	
		10C	475	
		12C	450	
Annealed CNT ⁴⁷	0.01-2	C/2	446	...
		1C	230	3.26
		2C	175	4
		5C	150	3.83
		10C	125	3.6
Multi-stacked CNT ⁴⁸	0.01-3	C/10	350	...
		C/5	312	...
		C/2	251	...
		1C	211	3.55
		2C	180	3.88
Acid heat treated CNT ⁴⁹	0.01-2	3C	150	...
		C/2	250	...
		1C	200	3.75
		2C	175	4
		5C	135	4.26
Vertical arrayed CNT ⁴⁰	0.01-3.5	10C	125	3.6
		1C	360	2.08
		2C	300	2.33
		3C	280	...
		10C	272	1.75
		36C	246	...

high irreversible capacity could be attributed to the intercalation of Li^+ into the interstitial spaces between the neighboring tubes and also outer surfaces of nanotubes. Thus, it may be considered that partial Li ions can be intercalated but cannot be deintercalated. Indeed, only Li^+ intercalated onto surfaces of the nanotubes can be easily deintercalated.⁴⁶

To further evaluate the rate performance of both the pristine-CNT and SPAPE-coated electrodes, galvanostatic charge-discharge measurements were carried out at different current densities. As shown in Figs. 7(c) and 7(d), after the cells were cycled at 1C rate for 50 cycles, the current densities were increased stepwise to 12C. It is clearly observed that the SPAPE-coated CNT delivers higher discharge capacity than pristine CNT for all C-rates (1C–12C). The SPAPE-coated CNT delivers a stable capacity of 700 mAh g^{-1} ($257 \mu\text{Ah cm}^{-2}$) at 2C, 575 mAh g^{-1} ($211 \mu\text{Ah cm}^{-2}$) at 5C, 475 mAh g^{-1} ($175 \mu\text{Ah cm}^{-2}$) at 10C, and 450 mAh g^{-1} ($166 \mu\text{Ah cm}^{-2}$) at 12C. The capacity can be recovered after cycling at fast C-rate over 110 cycles. Pristine CNT shows lower discharge capacities at all C-rates. For pristine CNT, it delivers a stable capacity of 440 mAh g^{-1} ($162 \mu\text{Ah cm}^{-2}$) at 2C, 390 mAh g^{-1} ($143 \mu\text{Ah cm}^{-2}$) at 5C, 340 mAh g^{-1} ($125 \mu\text{Ah cm}^{-2}$) at 10C, and 320 mAh g^{-1} ($118 \mu\text{Ah cm}^{-2}$) at 12C. The SPAPE-coated CNT reaches a higher reversible capacity of 750 mAh g^{-1} ($276 \mu\text{Ah cm}^{-2}$) compared to pristine CNT which delivers a reversible capacity of 450 mAh g^{-1} ($166 \mu\text{Ah cm}^{-2}$) after 110 cycles at 1C rate. When CNT tissues are conformally coated with a polymer electrolyte, the cycling performance could be improved ~67% at 1C rate over 110 cycles. These results show that conformal deposition via electropolymerization has a great benefit to enhance the electrochemical performance. The enhancement can be attributed to the larger electrode/electrolyte interface resulting in improved charge transport. The post-mortem analysis has been conducted on SPAPE-coated CNT electrodes to examine the morphology after 110 charge-discharge cycles performed at different C-rates (See Fig. S4, supplementary material). We found that the morphology after cycling is maintained, meaning that the functionalized electrode is capable of long-term charge-discharge cycles without structural failure.

A comparison with the literature is made and presented in Table I. The SPAPE-coated CNT shows better reversible capacity with a high increment factor (a gain of 1.75–4). Indeed, the results of the present work appear to be superior to the previous studies.^{40,47–49}

To highlight the above results, the better electrochemical performance of CNT-coated SPAPE can be attributed due to a better penetration of the polymer electrolyte onto the carbon nanotube surfaces, enhancing the electrolyte/electrode interface area.

To conclude, here, we reported on the electropolymerization of p-sulfonated poly(allyl phenyl ether) (SPAPE) into carbon nanotube tissues. We have shown that the high electrode/electrolyte interface area leads to enhanced electrochemical performance of SPAPE-coated CNT compared to that of pristine CNT tissues. Improvement of the capacity by 67% can be attained after electropolymerization of CNT tissues up to 12C. SEM observations show densified and bundled

CNTs are obtained after electropolymerization for 10 cycles. TEM imaging confirmed the presence of polymer layer outside the tubes on the order of 2–6 nm along the length of the carbon nanotubes. These results showed the CNT tissues coated with the polymer film utilizing solely an electrochemical method can be considered as a competitive anode material for the future generation of flexible Li-ion microbatteries. These findings are expected to stimulate and open up new avenues for the further research on this interesting topic.

See supplementary material for the cross-sectional view of the SPAPE-coated CNT tissues, EDX spectra of both pristine CNT tissues and SPAPE-coated CNT tissues, SEM images of CNT tissues after electropolymerization, and postmortem SEM images after long-term charge-discharge cycles.

The authors would like to thank the région Provence Alpes Côte d'Azur for the financial support. The SPAPE monomer for this study was kindly provided by The University of Rome Tor Vergata.

REFERENCES

- 1 J. B. Goodenough and K.-S. Park, *J. Am. Chem. Soc.* **135**, 1167 (2013).
- 2 J.-M. Tarascon and M. Armand, *Nature* **414**, 359 (2001).
- 3 H. Nishide and K. Oyaizu, *Science* **319**, 737 (2008).
- 4 B. Tripathi, P. Kumar, R. K. Katiyar, and R. S. Katiyar, *Appl. Phys. Lett.* **110**, 173902 (2017).
- 5 Y. Zhang, Y. Jiao, M. Liao, B. Wang, and H. Peng, *Carbon* **124**, 79 (2017).
- 6 L. Hu, H. Wu, F. La Mantia, Y. Yang, and Y. Cui, *ACS Nano* **4**, 5843 (2010).
- 7 J.-Z. Wang, S.-L. Chou, J. Chen, S.-Y. Chew, G.-X. Wang, K. Konstantinov, J. Wu, S.-X. Dou, and H. K. Liu, *Electrochem. Commun.* **10**, 1781 (2008).
- 8 S. Park, M. Vosguerichian, and Z. Bao, *Nanoscale* **5**, 1727 (2013).
- 9 M.-S. Wu, J.-T. Lee, P.-C. J. Chiang, and J.-C. Lin, *J. Mater. Sci.* **42**, 259 (2007).
- 10 W. Li, M. Li, Z. Yang, J. Xu, X. Zhong, J. Wang, L. Zeng, X. Liu, Y. Jiang, X. Wei, L. Gu, and Y. Yu, *Small* **11**, 2762 (2015).
- 11 B. Liu, J. Zhang, X. Wang, G. Chen, D. Chen, C. Zhou, and G. Shen, *Nano Lett.* **12**, 3005 (2012).
- 12 M.-S. Balogun, M. Yu, C. Li, T. Zhai, Y. Liu, X. Lu, and Y. Tong, *J. Mater. Chem. A* **2**, 10825 (2014).
- 13 T. Hu, X. Sun, H. Sun, M. Yu, F. Lu, C. Liu, and J. Lian, *Carbon* **51**, 322 (2013).
- 14 S. Y. Chew, S. H. Ng, J. Wang, P. Novák, F. Krumeich, S. L. Chou, J. Chen, and H. K. Liu, *Carbon* **47**, 2976 (2009).
- 15 K. Suemori, Y. Watanabe, and S. Hoshino, *Appl. Phys. Lett.* **106**, 113902 (2015).
- 16 M. Inaba, K. Ohara, M. Shibuya, T. Ochiai, D. Yokoyama, W. Norimatsu, M. Kusunoki, and H. Kawarada, *J. Appl. Phys.* **123**, 244502 (2018).
- 17 H. Shimoda, B. Gao, X. P. Tang, A. Kleinhammes, L. Fleming, Y. Wu, and O. Zhou, *Phys. Rev. Lett.* **88**, 015502 (2001).
- 18 H. Gao, F. Hou, X. Zheng, J. Liu, A. Guo, D. Yang, and Y. Gong, *Vacuum* **112**, 1 (2015).
- 19 S. Yang, J. Huo, H. Song, and X. Chen, *Electrochim. Acta* **53**, 2238 (2008).
- 20 M. Cabello, G. F. Ortiz, M. C. López, P. Lavela, R. Alcántara, and J. L. Tirado, *Electrochem. Commun.* **56**, 61 (2015).
- 21 J. F. M. Oudenhoven, L. Baggetto, and P. H. L. Notten, *Adv. Energy Mater.* **1**, 10 (2011).
- 22 N. Plylahan, M. Letiche, M. K. S. Barr, and T. Djenizian, *Electrochem. Commun.* **43**, 121 (2014).
- 23 I. V. Ferrari, M. Braglia, T. Djenizian, P. Knauth, and M. L. Di Vona, *J. Power Sources* **353**, 95 (2017).
- 24 S. Yehezkel, M. Auinat, N. Sezin, D. Starosvetsky, and Y. Ein-Eli, *Electrochim. Acta* **229**, 404 (2017).

- ²⁵S. Yehezkel, M. Auinat, N. Sezin, D. Starosvetsky, and Y. Ein-Eli, *J. Power Sources* **312**, 109 (2016).
- ²⁶W. Ren, D. Li, H. Liu, R. Mi, Y. Zhang, L. Dong, and L. Dong, *Electrochim. Acta* **105**, 75 (2013).
- ²⁷X. Xiang, Z. Huang, E. Liu, H. Shen, Y. Tian, H. Xie, Y. Wu, and Z. Wu, *Electrochim. Acta* **56**, 9350 (2011).
- ²⁸K. Edström, D. Brandell, T. Gustafsson, and L. Nyholm, *Electrochem. Soc. Interface* **20**, 41 (2011).
- ²⁹L.-F. Cui, L. Hu, J. W. Choi, and Y. Cui, *ACS Nano* **4**, 3671 (2010).
- ³⁰H. Hou, F. Vacandio, M. L. D. Vona, and P. Knauth, *J. Appl. Polym. Sci.* **129**, 1151 (2013).
- ³¹F. Wolfart, D. P. Dubal, M. Vidotti, R. Holze, and P. Gómez-Romero, *J. Solid State Electrochem.* **20**, 901 (2016).
- ³²N. Plylahan, M. Letiche, M. K. Samy Barr, B. Ellis, S. Maria, T. N. T. Phan, E. Bloch, P. Knauth, and T. Djenizian, *J. Power Sources* **273**, 1182 (2015).
- ³³N. A. Kyeremateng, F. Dumur, P. Knauth, B. Pecquenard, and T. Djenizian, *Electrochem. Commun.* **13**, 894 (2011).
- ³⁴C. A. Vlaic, S. Ivanov, R. Peipmann, A. Eisenhardt, M. Himmerlich, S. Krischok, and A. Bund, *Electrochim. Acta* **168**, 403 (2015).
- ³⁵N. A. Kyeremateng, F. Dumur, P. Knauth, B. Pecquenard, and T. Djenizian, *C. R. Chim.* **16**, 80 (2013).
- ³⁶J. Gao, J. Zhong, L. Bai, J. Liu, G. Zhao, and X. Sun, *Sci. Rep.* **4**, 3606 (2014).
- ³⁷Z. Liu, N. Bajwa, L. Ci, S. H. Lee, S. Kar, P. M. Ajayan, and J. Q. Lu, in *2007 IEEE International Interconnect Technology Conference* (IEEE, 2007), pp. 201–203.
- ³⁸B. Song, J. Yang, J. Zhao, and H. Fang, *Energy Environ. Sci.* **4**, 1379 (2011).
- ³⁹Y.-J. Xu, X. Liu, G. Cui, B. Zhu, G. Weinberg, R. Schlögl, J. Maier, and D. S. Su, *ChemSusChem* **3**, 343 (2010).
- ⁴⁰H. Zhang, G. Cao, Z. Wang, Y. Yang, Z. Shi, and Z. Gu, *Electrochim. Acta* **55**, 2873 (2010).
- ⁴¹L. He, C. Wang, X. Yao, R. Ma, H. Wang, P. Chen, and K. Zhang, *Carbon* **75**, 345 (2014).
- ⁴²L. G. Bulusheva, V. E. Arhipov, E. O. Fedorovskaya, S. Zhang, A. G. Kurenina, M. A. Kanygin, I. P. Asanov, A. R. Tsygankova, X. Chen, H. Song, and A. V. Okotrub, *J. Power Sources* **311**, 42 (2016).
- ⁴³J. Eom, D. Kim, and H. Kwon, *J. Power Sources* **157**, 507 (2006).
- ⁴⁴L. Zou, R. Lv, F. Kang, L. Gan, and W. Shen, *J. Power Sources* **184**, 566 (2008).
- ⁴⁵N. Yitzhack, M. Auinat, N. Sezin, and Y. Ein-Eli, *APL Mater.* **6**, 111102 (2018).
- ⁴⁶Z. Yang and H. Wu, *Solid State Ionics* **143**, 173 (2001).
- ⁴⁷S. Yoon, S. Lee, S. Kim, K.-W. Park, D. Cho, and Y. Jeong, *J. Power Sources* **279**, 495 (2015).
- ⁴⁸C. Kang, M. Patel, B. Rangasamy, K.-N. Jung, C. Xia, S. Shi, and W. Choi, *J. Power Sources* **299**, 465 (2015).
- ⁴⁹S. Lee, D. Cho, and Y. Jeong, *Fibers Polym.* **16**, 1600 (2015).